Delft University of Technology

Experimental study on drag coefficient of flexible vegetation under non-breaking waves

Reis, Rui A.; Fortes, Conceição J.E.M.; Rodrigues, José A.; Hu, Zhan; Suzuki, Tomohiro

Important note
To cite this publication, please use the final published version (if applicable).
Please check the document version above.

Research paper

Experimental study on drag coefficient of flexible vegetation under non-breaking waves

Rui A. Reis [a,b,*], Conceição J.E.M. Fortes [b], José A. Rodrigues [c,d], Zhan Hu [e,f,g], Tomohiro Suzuki [h,i]

[a] *CERIS, Instituto Superior Técnico, Universidade de Lisboa, Lisbon, Portugal*
[b] *Hydraulics and Environment Department, National Laboratory for Civil Engineering, Lisbon, Portugal*
[c] *Department of Mathematics, Instituto Superior de Engenharia de Lisboa, Instituto Politécnico de Lisboa, Lisbon, Portugal*
[d] *CIMA, Research Center in Mathematics and Applications, Évora, Portugal*
[e] *School of Marine Science, Sun Yat-sen University, and Southern Marine Science and Engineering Guangdong Laboratory, Zhuhai, China*
[f] *Guangdong Provincial Key Laboratory of Marine Resources and Coastal Engineering, Guangzhou, China*
[g] *Pearl River Estuary Marine Ecosystem Research Station, Ministry of Education, Zhuhai, China*
[h] *Flanders Hydraulics Research, Antwerp, Belgium*
[i] *Faculty of Civil Engineering and Geosciences, Delft University of Technology, Delft, the Netherlands*

ARTICLE INFO

ABSTRACT

Laboratory experiments of wave propagation over rigid and flexible vegetation fields, with the same configurations, were conducted to understand the effect of vegetation flexibility on the drag coefficient (C_D). The direct method and the least squares method (LSM), based on force and flow measurements, are applied to calculate the C_D in the experimental conditions. The formulations of both methods are extended to estimate the C_D for flexible vegetation cases. A video analysis was performed to account for the swaying motion. Typically, wave dissipation is lower for flexible than for rigid vegetation of the same configuration, under the same flow condition. Therefore, a proportional effect in the corresponding C_D results, obtained from common C_D calibration to wave dissipation without considering vegetation motion, is usually observed. However, the present results show that although the wave dissipation was 34% lower for flexible relative to rigid vegetation, the respective C_D values were close. C_D estimations considering vegetation motion and inertia suggest that C_D of flexible vegetation was up to 13% higher relative to rigid vegetation. Accounting for inertia reduced the C_D for rigid vegetation up to 7%, while raised the C_D for flexible vegetation up to 13%.

1. Introduction

Vegetation such as seagrass, seaweed, saltmarshes, and mangroves play an important role in the normal equilibrium of coastal environments. Over the past couple of decades, the wave dissipation that occurs when waves propagate over vegetation has been widely investigated and acknowledged. Nevertheless, it remains a challenge to quantify the wave-vegetation interactions involved (Anderson et al., 2011; Nepf, 2011; van Veelen et al., 2021).

Initial analytical models adopted a simpler bottom friction approach to estimate the wave dissipation by vegetation effect (e.g., Camfield, 1983; Möller et al., 1999; Price et al., 1968). Dalrymple et al. (1984) introduced a formulation for wave dissipation over vegetation fields following the linear wave theory, based on the drag force acting on a group of rigid cylinders (Morison et al., 1950). In this way, the physical detail and the complex structure of vegetation fields can be best accounted. Mendez and Losada (2004) extended this modelling approach and included the effects of varying depth, wave breaking, and narrow-banded random waves. Although the capability to simulate the wave propagation over vegetation via the drag force on rigid cylinders (or blades) was implemented in diverse types of numerical models (e.g., Cao et al., 2015; Suzuki et al., 2012), those depend on a key parameter, the drag coefficient (C_D), that cannot be directly measured (e.g., Anderson and Smith, 2014; Sánchez-González et al., 2011). Otherwise, numerical models that can reproduce the hydrodynamics around a cylinder will be necessary (e.g., Maza et al., 2015 for rigid vegetation; El Rahi et al., 2023 for flexible vegetation).

The vegetation C_D has been commonly estimated for a representative

---

vegetation field element by fitting the Mendez and Losada (2004) analytical force-based wave dissipation model (or similar formulation) to measured data of wave attenuation (calibration method). Thus, C_D acts as a calibration parameter of the model assumptions (e.g., assuming vegetation as rigid with no motion), that is adjusted to specific wave height reduction measured in the laboratory, or in the field (e.g., Jadhav et al., 2013; Ozeren et al., 2014).

Previously, for single rigid cylinders exposed to periodic flows, the drag (C_D) and inertia (C_M) coefficients have been determined based on force measurements using the Fourier analysis (Keulegan and Carpenter, 1958), and the least squares method (LSM) (Sumer and Fredsøe, 2006). Sarpkaya and Isaacson (1981) have shown from vast experiments on individual rigid cylinders under oscillatory flows that C_D approximately varied within the range from 0.5 to 2.5. However, a considerably higher C_D range, derived via the calibration method, can be found for diverse wave dissipation by vegetation conditions studied (Chen et al., 2018; Vuik et al., 2016). To investigate the design of bamboo structures for mangrove restoration, Gijón Mancheño et al. (2021) studied the C_D in arrays of rigid dense cylinders from force measurements, by means of the LSM. Based on flume experiments, Hu et al. (2014) calculated the C_D for individual vegetation field elements (cylinders) directly from wave force measurements, by evaluating the work done by the drag term of the force (direct method). Hu et al. (2014) and Chen et al. (2018) observed that the direct method led to less scattered C_D values compared to the commonly used calibration method. The C_D of vegetation under waves is more directly connected with the force applied than with the related wave dissipation. Therefore, the estimation methods based on the actual measured force may provide more accurate C_D results. Furthermore, they may help to eliminate potential modelling errors.

Natural coastal vegetation exposed to waves is commonly flexible (Feagin et al., 2011). Some studies reported that flexibility influences the amount of wave attenuation over vegetation and wave force on vegetation (e.g., Paul et al., 2016). From field measurements, Riffe et al. (2011) found that the wave dissipation through natural salt marsh vegetation was about half the dissipation expected for rigid vegetation. However, Augustin et al. (2009) found similar wave dissipation between rigid and flexible mimics. Mullarney and Henderson (2010), based on analytical modelling and field observations, found that the total dissipation for moderately flexible natural salt marsh stems was about 30% of the dissipation for equivalent rigid stems. Nevertheless, Luhar and Nepf (2016) experimentally observed that hydrodynamic wave forces generated by flexible blades may unusually exceed those generated by rigid blades of the same morphology. They proposed a physics-based numerical model for the wave-induced dynamics of flexible blades. Their model results suggested that C_D and C_M of a rigid-body may be used for a flexible body, if the relative body-normal velocity and acceleration are used to calculate the drag and added mass forces. Contrastingly, van Veelen et al. (2020) estimated the drag coefficient for flexible vegetation is up to 70% lower than for rigid vegetation in their flume tests that isolated the flexibility effect. Their C_D estimation was based on wave attenuation measurements (common calibration method) without considering the vegetation motion and inertia force. To further understand the relations between C_D of flexible and rigid vegetation, it is ideal/preferable that the calculation of C_D accounts for combined measured data of both in-field wave force (Hu et al., 2014) and vegetation motion (Asano et al., 1993; Bradley and Houser, 2009; Méndez et al., 1999) induced by the waves, as well as for the inertia force term.

In this study, the wave dissipation and C_D are investigated for vegetation fields exposed to wave conditions. As a novelty, the vegetation C_D is calculated based on in-field measurements of the force and vegetation motion, for the case of flexible vegetation under waves. Considering vegetation fields with same morphology under same wave flows, the influences of vegetation flexibility/motion and inertia on C_D is

further analysed. In summary, flume experiments of wave propagation over artificial vegetation fields were conducted that included a video analysis to the flexible vegetation motion. Vegetation fields constructed from cylinders that varied in flexibility only were analysed: rigid with no motion vs flexible with swaying motion. Two methods based on wave force measurements, the "direct method" (Hu et al., 2014) and the "least squares method (LSM)" (Sumer and Fredsøe, 2006), were applied to estimate the C_D in the experimental conditions. The direct method and LSM are extended to estimate the C_D of flexible vegetation case, based on measured data of the force and flow, combined with video analysed data of the vegetation motion. The estimations through the LSM considered the usually neglected inertia force deriving both C_D and C_M. Finally, the C_D results are analysed and compared between the two methods and different vegetation flexibilities.

2. Drag coefficient calculation

2.1. Direct method

For an individual vertical rigid cylinder under oscillatory flow propagating in the horizontal direction, the total time-varying horizontal force (F) is given by the Morison equation (Morison et al., 1950), according to:

$$F = \frac{1}{2} \rho \, d_v \, l_v \, C_D \, u(t) \, |u(t)| + \rho \, A_v \, l_v \, C_m \, a(t) + \rho \, A_v \, l_v \, a(t) \tag{1}$$

where t is the time, C_D is the drag coefficient, C_m is the hydrodynamic-mass coefficient, l_v is the length of the cylinder (i.e., height in a vertical posture), ρ ($=1000$ kg/m³) is the mass density of the water, d_v is the diameter of the cylinder, A_v is the base area of the cylinder given by $A_v = \pi/4 \, d_v^2$, a is the water flow horizontal acceleration, and u is the water flow horizontal velocity. On the right-hand side of Eq. (1), the first term is the horizontal drag force (F_D), and the summation of the horizontal hydrodynamic-mass force (second term) and the horizontal Froude-Krylov force (third term) equals the horizontal inertia force (F_I), such that:

$$F = F_D + F_I \tag{2}$$

The inertia coefficient (C_M) relates to C_m as follows:

$$C_M = C_m + 1 \tag{3}$$

Therefore, F (Eq. (1)) can be expressed according to:

$$F = \frac{1}{2} \rho \, d_v \, l_v \, C_D \, u(t) \, |u(t)| + \rho \, C_M \, A_v \, l_v \, a(t) \tag{4}$$

Hu et al. (2014) calculated the drag coefficient (C_D) for individual in-canopy rigid elements (wooden cylinders/rods) from force measurements in their experimental tests. Their C_D calculation method ("direct method") is taken directly from the measured total force applied (F_{meas}), evaluating the work done by the drag term of the force. Through the direct method, a wave period (T) averaged C_D of a rigid cylindrical vegetation element can be derived as follows:

$$C_D = \frac{2 \int_0^T F_{meas}(t) \, u(t) \, dt}{\rho \, d_v \, l_v \int_0^T u^2(t) \, |u(t)| \, dt} \tag{5}$$

2.1.1. Direct method for rigid vegetation

A slight change to Eq. (5) is made using the height of the cylinder underwater (h_v) instead of l_v, as follows:

$$C_D = \cfrac{2 \displaystyle\int_0^T F_{\text{meas}}(t)\, u(t)\, dt}{\rho\, d_{\text{v}} \displaystyle\int_0^T h_{\text{v}}(t)\, u^2(t)\, |u(t)|\, dt} \tag{6}$$

where h_{v} is defined as:

$$h_{\text{v}} = \begin{cases} l_{\text{v}}, & h + \eta(t) \geq l_{\text{v}} \\ h + \eta(t), & h + \eta(t) < l_{\text{v}} \end{cases} \tag{7}$$

η is the free-surface elevation, and h is the still water depth.

Compared to Eq. (5), Eq. (6) is preferable for vegetation of any submergence ratio (l_{v}/h) – holding for instants when water column (= $h + \eta(t)$) is lower than l_{v} – avoiding C_D being underestimated by taking l_{v} instead of the vegetation height (h_{v}) that, for every instant, is actually affected by the flow.

2.1.2. Direct method for flexible vegetation

For a flexible cylinder (i.e., that moves relative to the flow motion), the Morison Eq. (1) (valid for a rigid cylinder) can be written as follows (Sumer and Fredsøe, 2006):

$$F = \frac{1}{2}\, \rho\, d_{\text{v}}\, h_{\text{v}}(t)\, C_D\, u_r(t)\, |u_r(t)| + \rho\, A_{\text{v}}\, h_{\text{v}}(t)\, C_m\, a_r(t) + \rho\, A_{\text{v}}\, h_{\text{v}}(t)\, a(t) \tag{8}$$

with:

$$u_r = u(t) - u_{\text{v}}(t) \tag{9}$$

h_{v} is the height of the cylinder underwater, u_r is the horizontal velocity of the water flow relative to the vegetation motion, u_{v} is the horizontal velocity of the vegetation motion, and a_r is the horizontal acceleration of the water flow relative to the vegetation.

The C_D calculation through the direct method (Eq. (6)) is reformulated to flexible cylinders' case (first term of Eq. (8)), as follows:

$$C_D = \cfrac{2 \displaystyle\int_0^T F_{\text{meas}}(t)\, u_r(t)\, dt}{\rho\, d_{\text{v}} \displaystyle\int_0^T h_{\text{v}}(t)\, u_r^2(t)\, |u_r(t)|\, dt} \tag{10}$$

The C_D calculations performed for both rigid (Eq. (6)) and flexible vegetation (Eq. (10)) are over the successive waves analysed in each test data record.

2.2. Least squares method

Experimental force measurements may still be the most reliable source of information regarding the force coefficients (C_D, C_m and C_M). Two known techniques already applied to individual rigid cylinders in

$$\varepsilon^2 = \sum \left[F_{\text{pred}}(t) - F_{\text{meas}}(t) \right]^2 \tag{11}$$

is minimum.

2.2.1. LSM for rigid submerged vegetation

Based on the LSM (Sumer and Fredsøe, 2006), assuming F_{pred} is given by Eq. (1), and defining for convenience:

$$f_D = \frac{1}{2}\, \rho\, d_{\text{v}}\, l_{\text{v}}\, C_D \tag{12}$$

and

$$f_m = \rho\, A_{\text{v}}\, l_{\text{v}}\, C_m, \tag{13}$$

Eq. (11) becomes:

$$\varepsilon^2 = \sum \left[f_D\, u(t)\, |u(t)| + f_m\, a(t) + \rho\, A_{\text{v}}\, l_{\text{v}}\, a(t) - F_{\text{meas}}(t) \right]^2. \tag{14}$$

For ε^2 to be minimum:

$$\frac{\partial \varepsilon^2}{\partial f_D} = 0 \tag{15}$$

and

$$\frac{\partial \varepsilon^2}{\partial f_m} = 0. \tag{16}$$

Eqs. (15) and (16) lead, respectively, to:

$$f_D \left[\sum u^4(t) \right] + f_m \left[\sum u(t)\, |u(t)|\, a(t) \right] + \rho\, A_{\text{v}}\, l_{\text{v}} \left[\sum u(t)\, |u(t)|\, a(t) \right] = \sum u(t)\, |u(t)|\, F_{\text{meas}}(t) \tag{17}$$

and

$$f_D \left[\sum u(t)\, |u(t)|\, a(t) \right] + f_m \left[\sum a^2(t) \right] + \rho\, A_{\text{v}}\, l_{\text{v}} \left[\sum a^2(t) \right] = \sum a(t)\, F_{\text{meas}}(t) \tag{18}$$

After obtaining f_D and f_m by solving the system of Eqs. (17) and (18), the coefficients C_D and C_m are determined from Eqs. (12) and (13). C_M is obtained from C_m by Eq. (3).

2.2.2. LSM for rigid emergent vegetation

Assuming F_{pred} is calculated by Eq. (1), but replacing l_{v} by h_{v}, such that:

$$F_{\text{pred}} = \frac{1}{2}\, \rho\, d_{\text{v}}\, h_{\text{v}}(t)\, C_D\, u(t)\, |u(t)| + \rho\, A_{\text{v}}\, h_{\text{v}}(t)\, C_m\, a(t) + \rho\, A_{\text{v}}\, h_{\text{v}}(t)\, a(t), \tag{19}$$

through the LSM Eq. (11) becomes:

$$\varepsilon^2 = \sum \left[\frac{1}{2}\, \rho\, d_{\text{v}}\, h_{\text{v}}(t)\, C_D\, u(t)\, |u(t)| + \rho\, A_{\text{v}}\, h_{\text{v}}(t)\, C_m\, a(t) + \rho\, A_{\text{v}}\, h_{\text{v}}(t)\, a(t) - F_{\text{meas}}(t) \right]^2. \tag{20}$$

oscillatory flows, yielding approximate results, are the Fourier analysis (Keulegan and Carpenter, 1958; Sarpkaya and Isaacson, 1981) and the least squares method (LSM) (Sumer and Fredsøe, 2006). The LSM determines the force coefficients in such a way that the mean-squared difference between the predicted wave force on the cylinder F_{pred} (given by the Morison Eq. (1)) and the measured force F_{meas}:

Considering:

$$\zeta_D = \frac{1}{2}\, \rho\, d_{\text{v}}\, C_D \tag{21}$$

and

$$\zeta_m = \rho\, A_{\text{v}}\, C_m, \tag{22}$$

for ε^2 (Eq. (20)) to be minimum:

$$\frac{\partial \varepsilon^2}{\partial \zeta_D} = 0 \tag{23}$$

and

$$\frac{\partial \varepsilon^2}{\partial \zeta_m} = 0 \; . \tag{24}$$

Eqs. (23) and (24), respectively, lead to:

$$\zeta_D \left[\sum h_v{}^2(t)\, u^4(t) \right] + \zeta_m \left[\sum h_v{}^2(t)\, u(t)\, |u(t)|\, a(t) \right] + \rho\, A_v \left[\sum h_v{}^2(t)\, u(t)\, |u(t)|\, a(t) \right] = \sum h_v(t)\, u(t)\, |u(t)|\, F_{\text{meas}}(t) \tag{25}$$

and

$$\zeta_D \left[\sum h_v{}^2(t)\, u(t)\, |u(t)|\, a(t) \right] + \zeta_m \left[\sum h_v{}^2(t)\, a^2(t) \right] + \rho\, A_v \left[\sum h_v{}^2(t)\, a^2(t) \right] = \sum h_v(t)\, a(t)\, F_{\text{meas}}(t) \tag{26}$$

After obtaining ζ_D and ζ_m by solving the system of Eqs. (25) and (26), the coefficients C_D and C_m are determined from Eqs. (21) and (22). C_M is obtained through Eq. (3).

Note that the solution in Eqs. (25) and (26) hold for vegetation of any submergence ratio (l_v/h), valid for instants when the water column is lower than l_v.

2.2.3. LSM for flexible vegetation

The application of the LSM is extended to flexible vegetation case, considering F_{pred} as given by Eq. (8). Following the LSM, Eq. (11) becomes:

$$\varepsilon^2 = \sum \left[\frac{1}{2}\, \rho\, d_v\, h_v(t)\, C_D\, u_r(t)\, |u_r(t)| + \rho\, A_v\, h_v(t)\, C_m\, a_r(t) + \rho\, A_v\, h_v(t)\, a(t)\; - \; F_{\text{meas}}(t) \right]^2 \tag{27}$$

Considering the Eqs. (21) and (22), for ε^2 (Eq. (27)) to be minimum, Eqs. (23) and (24), respectively, lead to:

$$\zeta_D \left[\sum h_v{}^2(t)\, u_r{}^4(t) \right] + \zeta_m \left[\sum h_v{}^2(t)\, u_r(t)\, |u_r(t)|\, a_r(t) \right] + \rho\, A_v \left[\sum h_v{}^2(t)\, u_r(t)\, |u_r(t)|\, a(t) \right] = \sum h_v(t)\, u_r(t)\, |u_r(t)|\, F_{\text{meas}}(t) \tag{28}$$

and

$$\zeta_D \left[\sum h_v{}^2(t)\, u_r(t)\, |u_r(t)|\, a_r(t) \right] + \zeta_m \left[\sum h_v{}^2(t)\, a_r{}^2(t) \right] + \rho\, A_v \left[\sum h_v{}^2(t)\, a_r(t)\, a(t) \right] = \sum h_v(t)\, a_r(t)\, F_{\text{meas}}(t) \tag{29}$$

Solving the system of Eqs. (28) and (29) gives ζ_D and ζ_m. The coefficients C_D and C_m are determined from Eqs. (21) and (22).

Note that, like the C_D calculations through the direct method (Sections 2.1.1 and 2.1.2), the calculations using the LSM (Sections 2.2.1, 2.2.2 and 2.2.3) are over the successive waves analysed in each test data record.

3. Experimental tests

3.1. Flume setup

The laboratory experiments were conducted in the wave flume COI3 of the National Laboratory for Civil Engineering (LNEC). The flume is 33 m long with 1 m width at the beginning and 0.6 m at its end. The wavemaker is of piston type without active wave absorption. A 1/20 bottom slope, 0.3 m high, with an adjacent flat bottom extent of 3.18 m length, was constructed of concrete. Next to it, a 7.12 m long flat false bottom made of horizontally connected plywood boards was installed. On top of the false bottom, 5 m long (from $x = 21.45$–26.45 m) artificial vegetation fields were built from cylindrical elements/units that mimicked natural vegetation. On the opposite side of the wavemaker, a 1/6.3 slope of stones (≈ 7 cm average diameter) that promoted wave breaking was installed to dissipate the wave energy at the flume end. The lateral walls are made of concrete except for a transparent glass from $x = 21.20$–27.00 m (Fig. 1 top left).

Two types of artificial vegetation fields constructed from cylinders of different materials were tested: i) vegetation fields made of rigid pine wood cylinders, and ii) vegetation fields built from flexible (and buoyant) cylinders made of sponged rubber. The two vegetation element
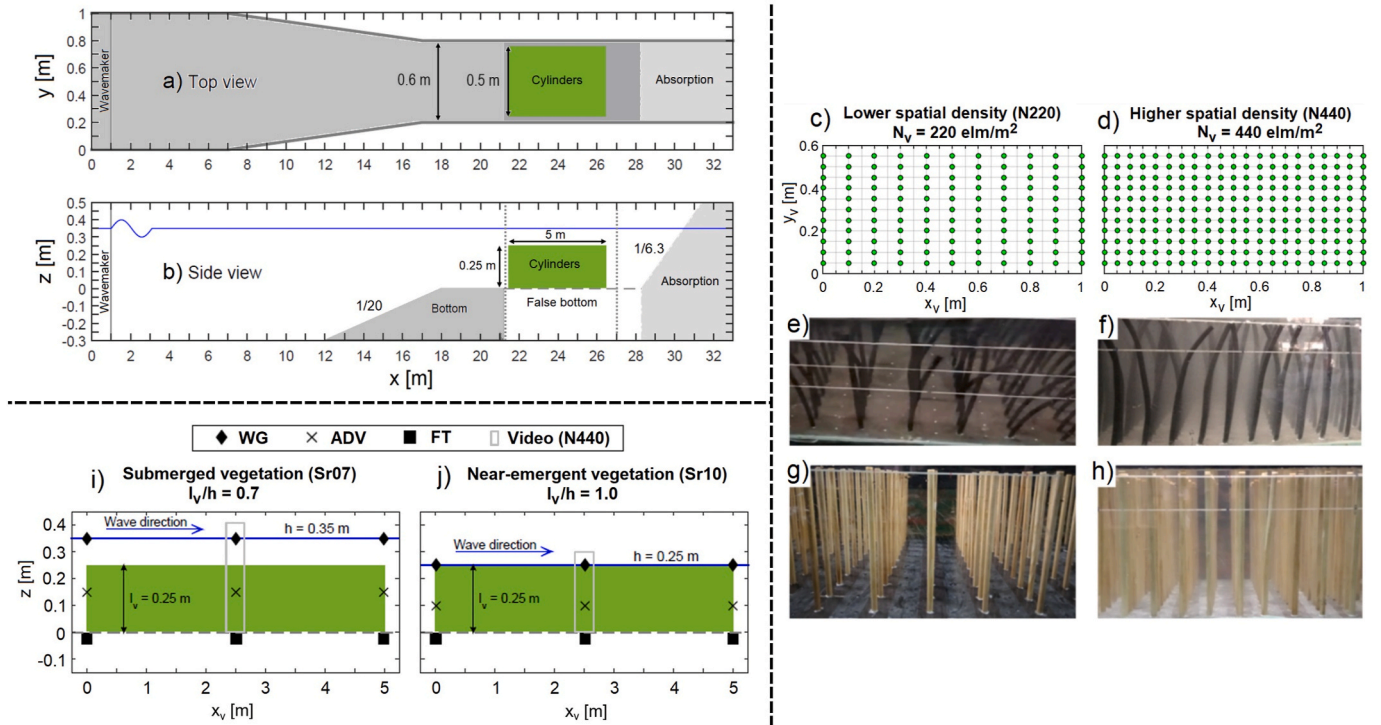
Fig. 1. Wave flume layout schematisation (**top left**): **a)** top view, and **b)** side view.Top view sketch of the tested vegetation spatial densities (N_v) (**on the right**): **c)** lower density (N220) with N_v = 220 elm/m², and **d)** higher density (N440) with N_v = 440 elm/m². Side views of vegetation layouts (also **on the right**): **e)** flexible cylinders in lower density N220, **f)** flexible cylinders in higher density N440, **g)** rigid cylinders in lower density N220, and **h)** rigid cylinders in higher density N440. Locations of the measurements performed with wave gauges (WG), acoustic Doppler Velocimeter (ADV), and force transducer (FT), and of the video records (**bottom left**): **i)** submerged vegetation case (Sr07) with l_v/h = 0.7, and **j)** near-emergent vegetation case (Sr10) with l_v/h = 1.0.

types (rigid and flexible) had the same dimensions, i.e., the same diameter (d_v = 0.01 m) and height in a vertical posture (l_v = 0.25 m), so they differed mainly in flexibility. In the present study, the vegetation is considered flexible or rigid if, under the same flow conditions, it is deformable (i.e., moves relative to the flow – sways) or it remains static, respectively. The flexural rigidity can be determined by the product of

the Young's elastic modulus (E) and the second moment of area ($I = \pi d_v^4/64$, for a filled circle), EI, which gives a measure of the overall flexibility of the vegetation element (Rupprecht et al., 2015). Since the two types of vegetation elements used had the same d_v = 0.01 m, the higher the E value, the less flexible the vegetation type. The E of the materials was determined from tensile stress experimental tests, using an

Table 1
Characteristics of the tested vegetation elements.

Vegetation element	Material	d_v [m]	l_v [m]	ρ_v * [kg/m³]	E [MPa]	EI [N m²]	B [#] [-]
Rigid cylinder	Pine wood	0.01	0.25	310	13200	6.5	–
Flexible cylinder	Sponged rubber	0.01	0.25	290	0.82	4.0×10^{-4}	21

* ρ_v is the mass density of the vegetation element; [#] $B = (\rho - \rho_v)\, g\, \pi\, d_v^2\, l_v^3\, (4\, EI)^{-1}$ is the buoyancy parameter, which may be relevant for flexible vegetation case (Luhar and Nepf, 2011; Luhar et al., 2017), where ρ is the mass density of the water (=1000 kg/m³) and g is the gravitational acceleration (=9.81 m/s²).

Table 2
Regular wave conditions tested alongside hydrodynamic and dimensionless parameters *.

Test ID	T [s]	h [m]	λ [m]	H_0 [m]	u_c [m/s]	H_0/h [#] [-]	kh [-]	Ur [-]	Re [-]	KC [-]	Fr [-]
Sr07_T14_H09	1.4	0.35	2.28	0.09	0.15	0.25	0.964	10.92	1536	22	0.08
Sr07_T14_H11	1.4	0.35	2.28	0.11	0.19	0.32	0.964	13.35	1917	27	0.10
Sr07_T14_H15	1.4	0.35	2.28	0.15	0.29	0.44	0.964	18.21	2858	40	0.15
Sr07_T14_H16	1.4	0.35	2.28	0.16	0.30	0.46	0.964	19.42	3017	42	0.16
Sr07_T20_H08	2.0	0.35	3.49	0.08	0.17	0.23	0.631	22.66	1725	34	0.09
Sr07_T20_H10	2.0	0.35	3.49	0.10	0.22	0.29	0.631	28.33	2156	43	0.12
Sr07_T20_H14	2.0	0.35	3.49	0.14	0.31	0.39	0.631	39.66	3098	62	0.17
Sr07_T20_H15	2.0	0.35	3.49	0.15	0.37	0.44	0.631	42.49	3687	74	0.20
Sr10_T14_H08	1.4	0.25	2.00	0.08	0.20	0.32	0.784	20.55	2022	28	0.13
Sr10_T14_H10	1.4	0.25	2.00	0.10	0.26	0.40	0.784	25.69	2639	37	0.17
Sr10_T14_H12	1.4	0.25	2.00	0.12	0.30	0.47	0.784	30.83	3015	42	0.19
Sr10_T14_H13	1.4	0.25	2.00	0.13	0.32	0.54	0.784	33.40	3248	45	0.21

* The values of the parameters are at the front-edge position (x_v = 0 m) in the control tests with no vegetation; [#] H_0/h is the relative wave height to water depth at the vegetation front-edge with H_0 the wave height at the front-edge.
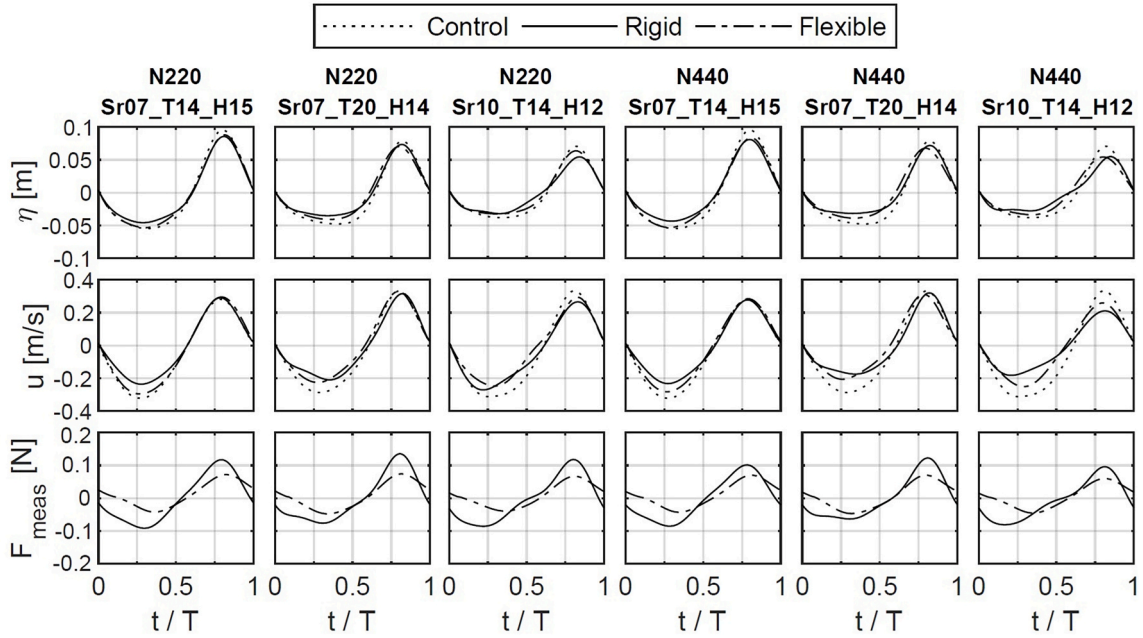
Fig. 2. Ensemble phase averaged data, at halfway position ($x_v = 2.5$ m), for conditions Sr07_T14_H15, Sr07_T20_H14, and Sr10_T14_H12 in rigid vegetation, flexible vegetation, and control tests. **Top row:** surface elevation (η) from WG. **Midlle row:** horizontal water flow (u) from the ADV. **Bottom row:** horizontal force from the FT (F_{meas}).
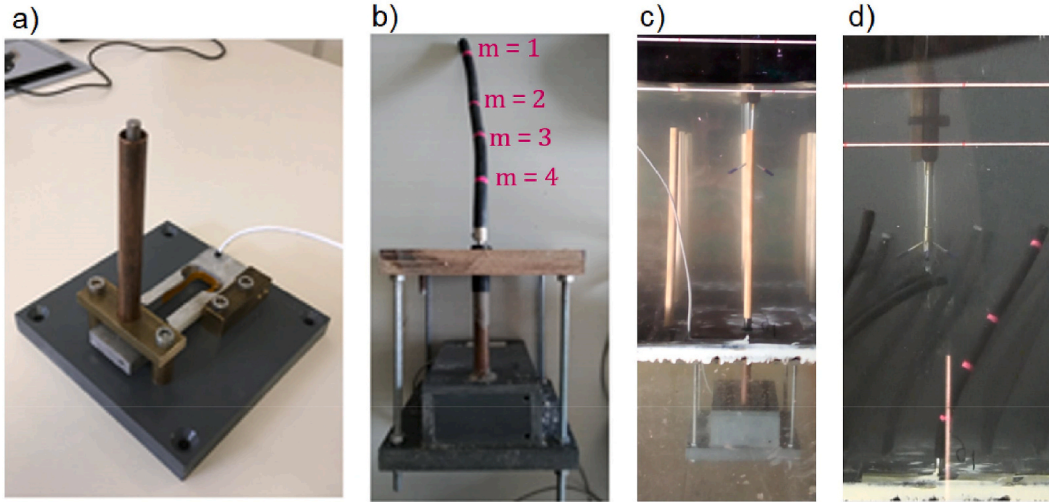

Fig. 3. **a)** photo showing the inside of the FT instrument; **b)** photo of the FT instrument connected to the flexible target cylinder with magenta marks; **c)** photo of the FT connected to a rigid cylinder, positioned at $x_v = 2.5$ m, during wave tests with rigid vegetation; **d)** cropped video frame of a video recording the marked target cylinder, while swaying during a wave test with flexible vegetation.

INSTRON 4302 mechanical machine, to both rigid and flexible vegetation elements (Table 1).

The vegetation fields covered a 5 m long by 0.5 m wide area of regularly distributed cylindrical elements (Fig. 1 top left). Two different vegetation spatial densities (N_v, expressed in the number of vegetation elements per horizontal area, elm/m²) were tested: a) lower density case (N220) with $N_v = 220$ elm/m², and b) higher density case (N440) with N_v m/m² (Fig. 1 on the right). These tested vegetation spatial densities corresponded to relative frontal areas $l_v d_v N_v$ (van Veelen et al., 2020) of 0.55 and 1.10.

3.2. Wave-vegetation conditions

The experimental tests complied with twelve regular wave conditions (Table 2). Two still water depths, $h = 0.35$ m and $h = 0.25$ m, and

two wave periods, $T = 1.4$ s (T14) and $T = 2.0$ s (T20), were tested. Reference/control tests without vegetation ($N_v = 0$ elm/m²) were taken before conducting the tests with the different vegetation fields. Note that, for all the wave tests (with and without vegetation), wave breaking (Hu et al., 2022) only occurred in the end of the flume at the wave absorption zone (Fig. 1 top left). Each test had a duration of 3 min. Around 60 fully developed regular waves were analysed in the tests with waves of $T = 1.4$ s (T14), and around 40 in the tests with waves of $T = 2.0$ s (T20).

The wave height H is calculated through zero down crossing method, as the average of the wave heights analysed from each wave gauge (WG) data record (Section 3.3). The characteristic horizontal flow velocity (u_c) is taken as the amplitude of the horizontal orbital wave velocity (u_w), defined as (Hu et al., 2014):
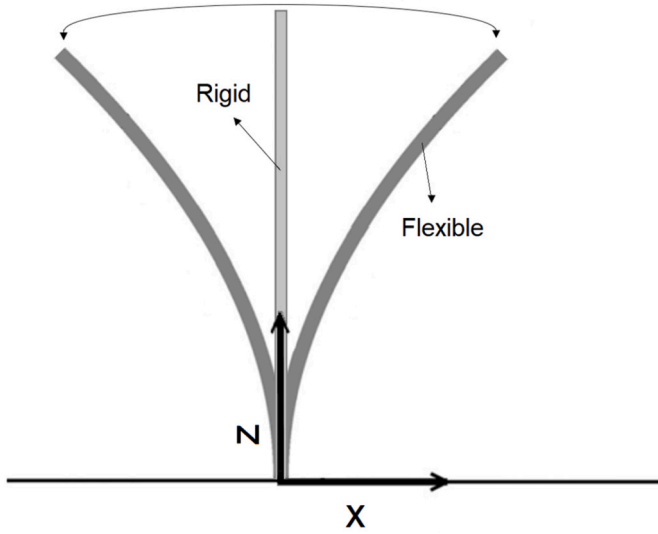
Fig. 4. Sketch of an ideal swaying motion of the tested flexible vegetation elements.

$$u_c = u_w = \frac{1}{2}\left(u_{\max} - u_{\min}\right) \tag{30}$$

where $u_{\max}$ and $u_{\min}$ were obtained as the average among the maximum and minimum horizontal flow velocities for the waves analysed in each acoustic Doppler velocimeter (ADV) data record at $z \approx h/2$ (Section 3.3).

The dimensionless depth, kh, was obtained by the Hunt (1979) formula (Dean and Dalrymple, 1991), where k is the wave number. Since h is a known experimental condition, k is derived from dividing kh by h. $\lambda = 2\pi/k$ is the wavelength, $Ur = H\lambda^2/h^3$ is the Ursell number, $Re = u_c d_v/\nu$ is the Reynolds number with ν the kinematic viscosity of the water ($=10^{-6}$ m^2/s), $KC = u_c T/d_v$ is the Keulegan-Carpenter number (Keulegan and Carpenter, 1958), and $Fr = u_c /\sqrt{g\,h}$ is the Froude number (Table 2).

The tested still water depths, $h = 0.35$ m and $h = 0.25$ m, corresponded to two tested submergence ratios (l_v/h), i.e., fractions of the vegetation occupation in the still wter depth (e.g., Koftis et al., 2013): a) submerged vegetation (Sr07) with $l_v/h = 0.7$, and b) near-emergent vegetation (Sr10) with $l_v/h = 1.0$ (Fig. 1 bottom left).

Wave-vegetation interactions are characterised by the dimensionless parameters Cauchy number $Ca = \rho\, u_c^2\, d_v\, l_v^3/EI$, being the ratio between wave forces and vegetation stiffness, and ratio between vegetation length and wave excursion $L = 2\pi\, l_v\, (u_c\, T)^{-1}$ (Luhar et al., 2017; van Veelen et al., 2021). In the experiments, accounting for the reference conditions in Table 2, the Ca range was 0.0005–0.0033 (rigid vegetation) and 8.8–53.5 (flexible vegetation), and the L range was 2.13–7.30.

3.3. Measurements and analysis

In-phase synchronised measurements were performed of i) the free-surface elevation (η) using resistive wave gauges (WG), ii) the horizontal water particle velocity (u) with a Nortek Vectrino acoustic Doppler velocimeter (ADV), and iii) the horizontal force (F_{meas}) on individual vegetation elements with a force transducer (FT). The sampling frequency was 50 Hz for all instruments. The measurements were taken at three coincident flume cross-sections along the vegetation fields: front-edge ($x_v = 0$ m), halfway ($x_v = 2.5$ m) and back-edge ($x_v = 5$ m) (Fig. 1 bottom left and Fig. 2). The vertical positions of the ADV flow measurements (u), $z = 0.15$ m for the submerged case and $z = 0.1$ m for the near-emergent case, approximately coincide with half of the water depth, at which the velocity roughly equals the depth-average velocity in the vegetation canopy, when the submergence ratio l_v/h (0.7 and 1 in this study) is high (Chen et al., 2018). The FT measured the total horizontal wave force (F_{meas}) applied to individual vegetation elements (Fig. 3a, b, and c) positioned next to the lateral glass ($y_v = 0.05$ m). The ADV and FT devices were moved between measurement locations (front-edge, halfway and back-edge) while repeated tests of each wave condition (Table 2) were performed. Measurements of η (WG) and u (ADV) were also taken in the control tests with no vegetation.

It is perceptible a general decrease in the wave height (Fig. 2 top row) and orbital wave velocity (Fig. 2 middle row) from the control tests to the vegetation tests. Also, a decrease in the force from rigid to flexible case is clear. The variations in u for rigid vegetation (pronounced in Sr10_T14_H12 case) are possibly due to a stronger downwash flow disturbing the flow at the measuring depth.

The wave height H was obtained at the front-edge, halfway, and back-edge of the vegetation fields (Fig. 1 bottom left) both for the tests with vegetation and without vegetation (Section 4.1).

The force transducer (FT) instrument (Bouma et al., 2005; Hu et al., 2014; Infantes et al., 2011) was developed at the Flanders Hydraulics. The FT consisted of a load cell connected to a rod metal bar, respectively
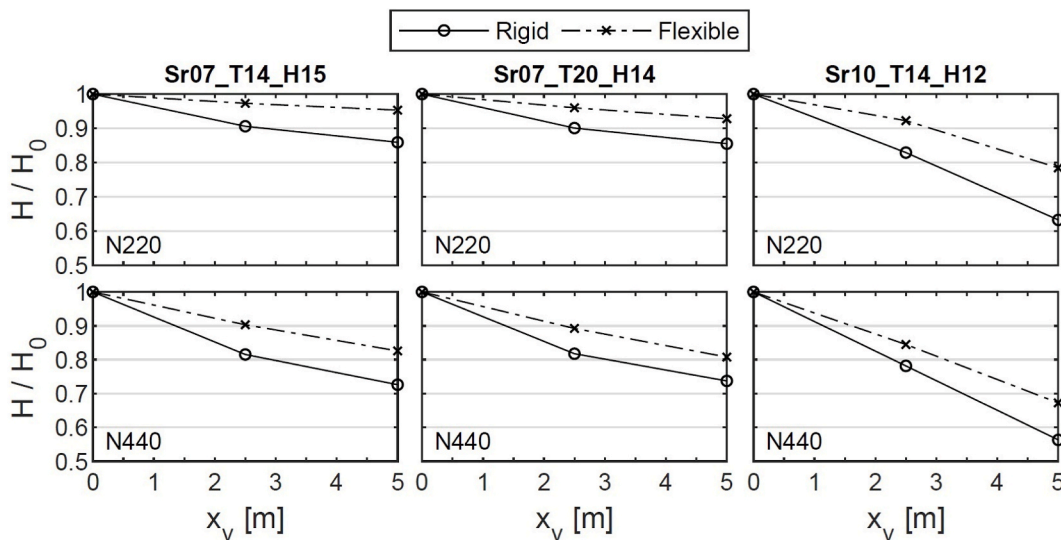

Fig. 5. Wave dissipation by vegetation for the tests Sr07_T14_H15 (left column), Sr07_T20_H14 (middle column) and Sr10_T14_H12 (right column) (for meaning of the tests ID and conditions, see Table 2 and Fig. 1).
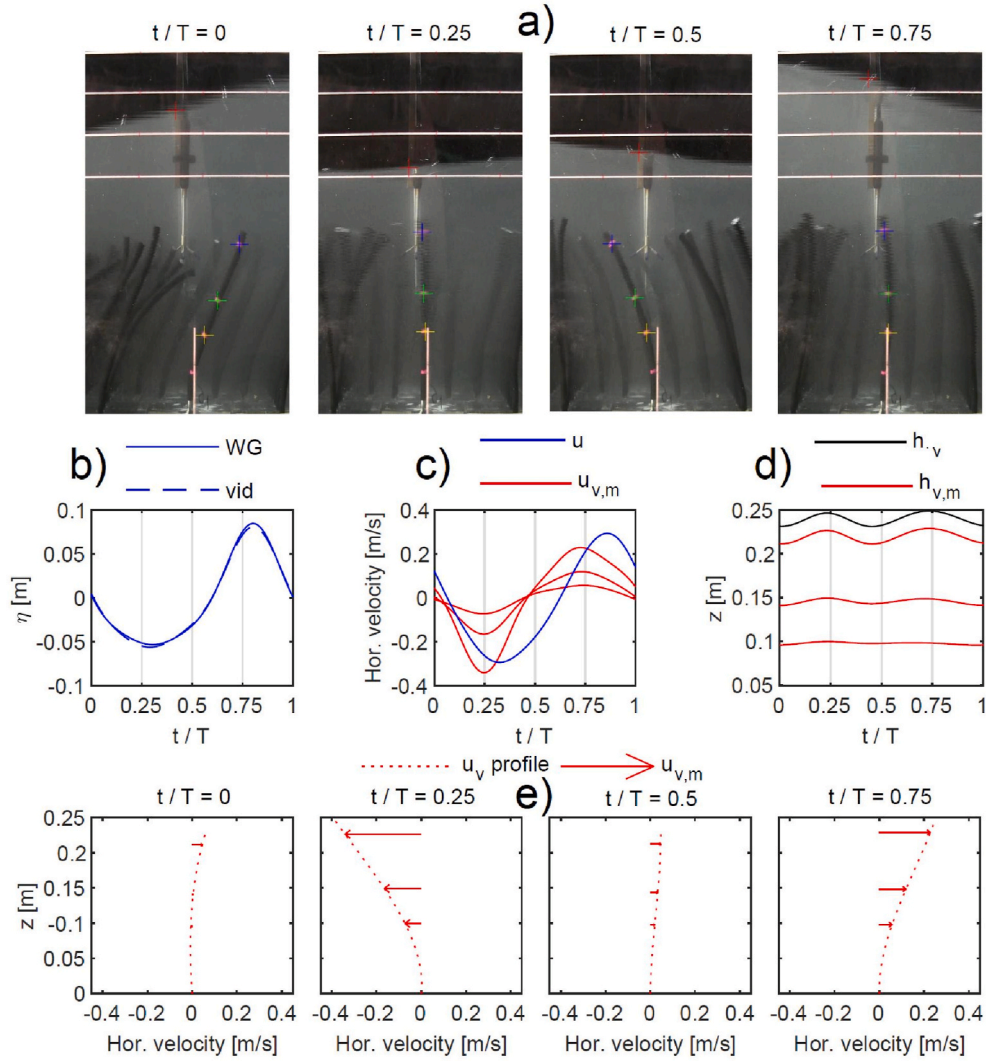
Fig. 6. Timely adjusted data results obtained from the video analysis (η, $h_{v,m}$, $u_{v,m}$, h_v, and u_v vertical profile) along with corresponding synchronised data from the instruments WG (η) and ADV (u), for a single wave (the first wave analysed in the record) of the test Sr07_T14_H15: **a)** video frames (of the instants $t/T = 0$, $t/T = 0.25$, $t/T = 0.5$, and $t/T = 0.75$) showing the video analysis tracking markers of the target cylinder magenta marks (blue, green, and yellow plus sign markers) and of the free-surface elevation (red plus sign marker). **b)** free-surface elevation (η) obtained from the WG and from the video analysis (vid). **c)** horizontal flow velocity u (ADV), and horizontal velocity of the magenta marks $m = 1$ to $m = 3$ ($u_{v,m}$) obtained from the video analysis. The red lines with highest and lowest amplitudes correspond respectively to $u_{v,1}$ and $u_{v,3}$. **d)** height of the magenta marks $m = 1$ to $m = 3$ ($h_{v,m}$) and total height of the target cylinder underwater (h_v), both calculated through the video analysis. The red lines with highest and lowest amplitudes correspond respectively to $h_{v,1}$ and $h_{v,3}$. **e)** $u_{v,m}$ of magenta marks $m = 1$ to $m = 3$ (for the instants $t/T = 0$, $t/T = 0.25$, $t/T = 0.5$, and $t/T = 0.75$) and u_v vertical profile, both calculated through the video analysis. The red arrows with highest and lowest magnitudes correspond respectively to $u_{v,1}$ and $u_{v,3}$. The data is for the N440 vegetation spatial density at halfway the vegetation field ($x_v = 2.5$ m).

inside a PVC box and a hollow metal tube for flow disturbance protection. The bar was connected to individual rigid and flexible vegetation elements via a customised metal piece. The FT was placed in the false bottom, fixed and levelled to the plywood boards (Fig. 3). The voltage output of the FT varied linearly with the force exerted on it. The FT working range was from -1.5 N to 1.5 N. The measured forces (F_{meas}) in the wave tests ranged from -0.19 N in the opposite wave direction to 0.23 N in the wave direction.

During the experimental tests, while the rigid cylinders remained in an upright static posture when exposed to the wave force, the flexible cylinders exhibited a swaying movement responding to the wave flow. The swaying motion of flexible vegetation under waves is characterised by excursions in the wave direction as a response to the wave crests, and excursions in the opposite wave direction as a reaction to the wave troughs (Fig. 4).

For the wave tests with flexible vegetation in the higher spatial

density (N440), videos were simultaneously recorded (with a camera Canon LEGRIA HFM56), along with the in-phase synchronised measurements (WG, ADV and FT) (Fig. 1 bottom left), capturing (Fig. 3d) both the motion of the flexible vegetation element (target cylinder) connected to the FT and the free-surface elevation (η) at halfway the vegetation field ($x_v = 2.5$ m). The recorded target cylinder was marked in magenta colour with luminescent nail polish of colour magenta. Considering the flexible target cylinder in a straight vertical posture, the magenta marks $m = 1$ (mark 1) to $m = 4$ (mark 4) were placed at $z = 0.92$ $l_v = 23$ cm, $z = 0.6$ $l_v = 15$ cm, $z = 0.4$ $l_v = 10$ cm, and $z = 0.2$ $l_v = 5$ cm (from top to bottom) (Fig. 3b).

A video tracking analysis was implemented (using MATLAB 2018a) to estimate the free-surface elevation (η) and the motion of the magenta marks on the target flexible cylinder, at $x_v = 2.5$ m, for the tests with vegetation spatial density N440 (Section 4.2).
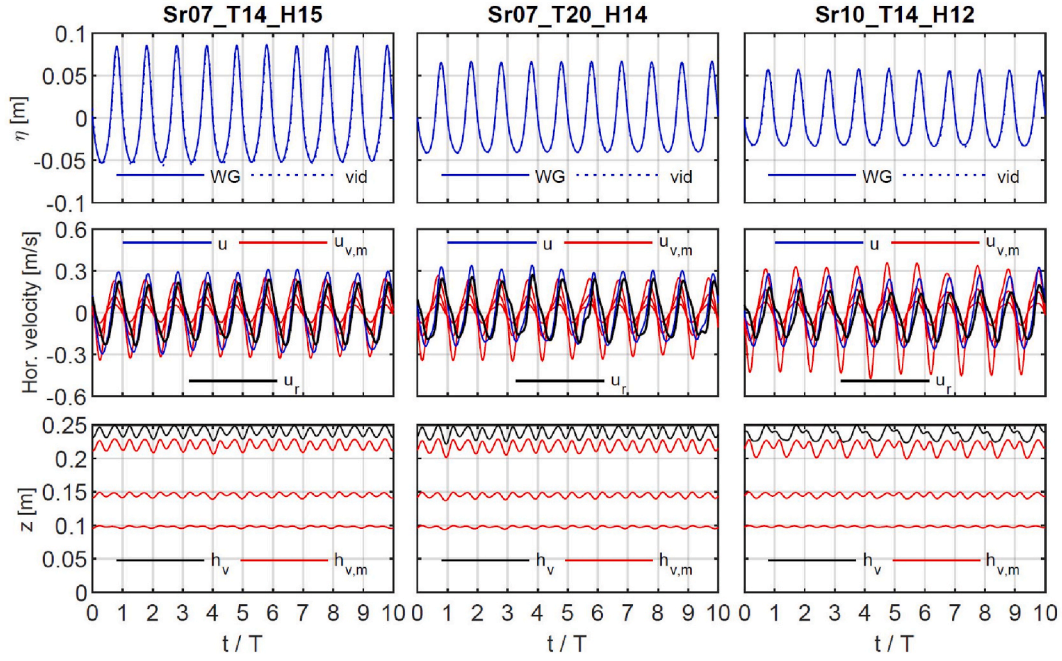
Fig. 7. Timely adjusted data obtained based on the video analysis (η, $h_{v,m}$, $u_{v,m}$, u_r, and h_v) along with corresponding synchronised data from the instruments WG (η) and ADV (u), for the first ten analysed waves of the tests Sr07_T14_H15 (left column), Sr07_T20_H14 (middle column), and Sr10_T14_H12 (right column). **Top row:** free-surface elevation (η) obtained from the WG and from the video analysis (vid). **Middle row:** horizontal flow velocity u (ADV), and horizontal velocity of the magenta marks $m = 1$ to $m = 3$ ($u_{v,m}$) and velocity of the water flow relative to the vegetation motion (u_r) both obtained based on the video analysis. The red lines with highest and lowest amplitudes correspond respectively to $u_{v,1}$ and $u_{v,3}$. **Bottom row:** height of the magenta marks $m = 1$ to $m = 3$ ($h_{v,m}$) and total height of the target cylinder underwater (h_v), both obtained based on the video analysis. The red lines with highest and lowest amplitudes correspond respectively to $h_{v,1}$ and $h_{v,3}$. The data is for the N440 vegetation spatial density at halfway the vegetation field ($x_v = 2.5$ m).

4. Results and discussion

4.1. Wave dissipation by vegetation

Normalised wave heights H/H_0 were obtained for each test condition at the front-edge, halfway, and back-edge of the vegetation fields. To consider only the vegetation effect on wave dissipation (Fig. 5) avoiding other factors (like bottom and sidewall friction), the differences between wave gauges obtained in the control tests were subtracted from those in the tests with vegetation (e.g., Augustin et al., 2009).

The wave dissipation over the length ($=5$ m) of the vegetation fields was calculated as the percentage of the wave height (H) reduction, ($H_0 - H_5)/H_0 \times 100$, where H_0 and H_5 are the H at the front-edge ($x_v = 0$ m) and back-edge ($x_v = 5$ m) positions. It was observed that the wave dissipation was higher for the higher vegetation spatial density case (N440), than for the lower spatial density case (N220), as expected. In average values, the wave dissipation percentage was 73% higher for N440 relative to the N220 case. The wave dissipation was lower for flexible vegetation than for rigid vegetation, likely due to the lower resistance of the flexible plants against the wave force compared to rigid plants. On average, the wave dissipation percentage was 34% lower for flexible vegetation relative to rigid vegetation. The wave dissipation percentage for the near-emergent vegetation case (Sr10, $l_v/h = 1.0$) was on average 118% higher relative to the submerged vegetation case (Sr07, $l_v/h = 0.7$). This increase in dissipation is related to the influence of the vegetation on the wave flow (and force) becoming closer to the water surface (when the relative portion of the vegetation in the water column is higher) where the wave orbital velocities and the turbulent kinetic energy are higher.

4.2. Vegetation motion

Based on the video analysis, timely adjusted data in-phase with the measured instrumental data (WG, ADV and FT), at 50 Hz frame frequency, was obtained of: i) the free-surface elevation (η) at $x_v = 2.5$ m, ii) the height of the magenta marks $m = 1$ to 3 on the target cylinder ($h_{v,1}$, $h_{v,2}$, and $h_{v,3}$), and iii) the horizontal velocities of the magenta marks $m = 1$ to 3 on the target cylinder, $u_{v,1}$, $u_{v,2}$, and $u_{v,3}$ (Fig. 6a, b, c, and d).

The results of free-surface elevation (η) obtained through the video analysis were quite close to the ones obtained through the WG measurements (Fig. 6b, and Fig. 7 top row) with average and maximum RMSE estimation scores of 0.002 m and 0.004 m. A phase difference between u and $u_{v,m}$ was observed with the excursions of the target cylinder in the wave direction being slower than the wave crests and the excursions in the opposite wave direction being faster than the wave troughs (Fig. 6c, and Fig. 7 middle row). The height of the target flexible cylinder underwater (h_v) (important to quantify the frontal area of vegetation that constrains the wave flow and resists the wave force) was estimated (black line in Fig. 6d) based on the mark 1 motion ($h_{v,1}$) and also (for near-emergent vegetation case) on the free-surface elevation (η) (i.e., on the water column $= h + \eta$), both obtained through the video analysis. Note that for higher submergence ratios (l_v/h), if the vegetation is flexible and buoyant (this study case), the movement of the vegetation (velocity and height of the vegetation top) can be directly influenced by the free-surface elevation (η) (i.e., influenced by the change of the water column $= h + \eta$). For some instants in the near-emergent case, h_v and $h_{v,1}$ approximate to the water column and to each other so that $h_v \approx h_{v,1} \approx h + \eta$ (the black line, h_v, gets closer to the top red line, $h_{v,1}$ – Fig. 7 bottom
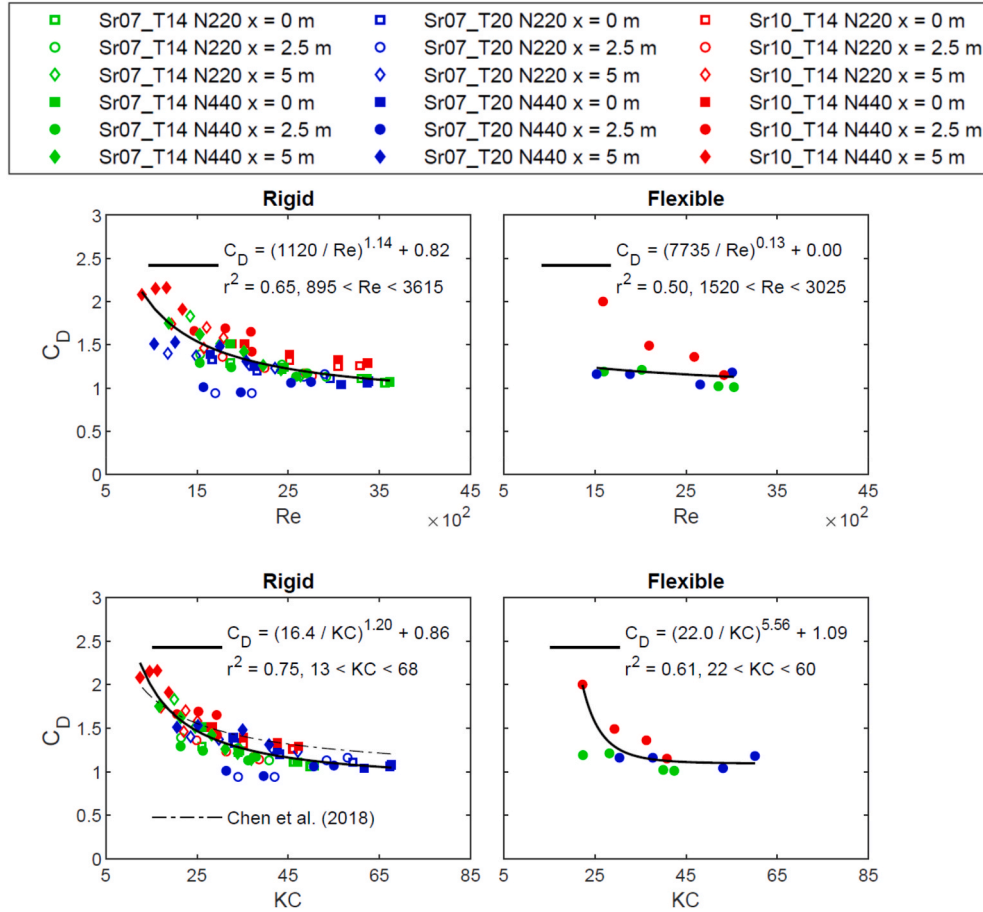
Fig. 8. C_D-Re (on top) and C_D-KC (at the bottom) empirical relations for C_D results obtained through the direct method ($C_{D,\text{direct}}$) in the rigid (left) (Eq. (6)) and flexible (right) (Eq. (10)) vegetation tests. Curve fittings (solid lines) of Eqs. (33) and (34) to the C_D-Re and C_D-KC results (markers) with derived equations, coefficent of determination (r^2), and ranges of Re and KC. C_D-KC relation obtained in Chen et al. (2018) (bottom left).

row, right column (Sr10_T14_H12 case)). A time-varying u_v vertical profile (Fig. 6e) was obtained at each time instant with a 0.001 m vertical resolution by spline cubic interpolation and extrapolation from the bottom ($z = 0$ m, $u_v = 0$ m/s) to the very top of the target flexible cylinder ($z = h_v$), taking the data ($h_{v,m}$ and $u_{v,m}$) of the marks 3, 2 and 1. Note that the motion of the mark $m = 4$ (mark 4) was not analysed, and according to video observations it was always minimal.

The velocity of the water flow relative to the vegetation motion (u_r), important to quantify how much the vegetation is conditioning/resisting the wave flow, was obtained (Fig. 7 middle row) by Eq. (9) considering the u (ADV) data, and the velocity of the vegetation movement (u_v) calculated as the average of the u_v vertical profile obtained (Fig. 6e).

4.3. Drag coefficient

4.3.1. C_D empirical relations

The dependency relation of drag coefficient (C_D) for wave forces applied on isolated cylinders with the Reynolds (Re) and Keulegan-Carpenter (KC) numbers is well known (e.g., Morison et al., 1950; Keulegan and Carpenter, 1958; Sumer and Fredsøe, 2006). Several studies (e.g., Anderson and Smith, 2014; Ozeren et al., 2014; Sánchez-González et al., 2011) have verified as well close dependency relations between wave force-related C_D with both Re and KC numbers in the case of waves propagating over artificial and real vegetation fields.

Re and KC are given as follows:

$$Re = u_c \, d_v / \nu \tag{31}$$

$$KC = u_c \, T / d_v \tag{32}$$

Based on the experimental tested conditions, new C_D-Re and C_D-KC empirical relations between C_D results and corresponding characteristic values of Re and KC were obtained, by finding the best fit through LSM of the following equations (Kobayashi et al., 1993) to the C_D-Re and C_D-KC results:

$$C_D = \left(\frac{a}{Re}\right)^b + c \tag{33}$$

$$C_D = \left(\frac{a}{KC}\right)^b + c \tag{34}$$

where a, b and c are fitted coefficients.

4.3.2. C_D via direct method

C_D results were calculated through the direct method ($C_{D,\text{direct}}$) using Eq. (6) (rigid vegetation) and (10) (flexible vegetation), based on the F_{meas} (FT) and u (ADV) data. For the rigid vegetation case the η (WG) data (Section 3.3) was considered, while for the flexible vegetation case the η, h_v, and u_r data were given through the video analysis (Section 4.2).

C_D-Re and C_D-KC empirical relations (Section 4.3.1) were obtained for the $C_{D,\text{direct}}$ results. Chen et al. (2018) also derived a C_D-KC relation (Fig. 7d in Chen et al., 2018), based on C_D results of Hu et al. (2014) calculated from direct method for rigid vegetation (cylinders/rods) under pure wave conditions. Similar trend and magnitude are found for the C_D-KC relation derived in this study compared to theirs (Fig. 8 bottom left). The slight differences between Chen et al. (2018) and this
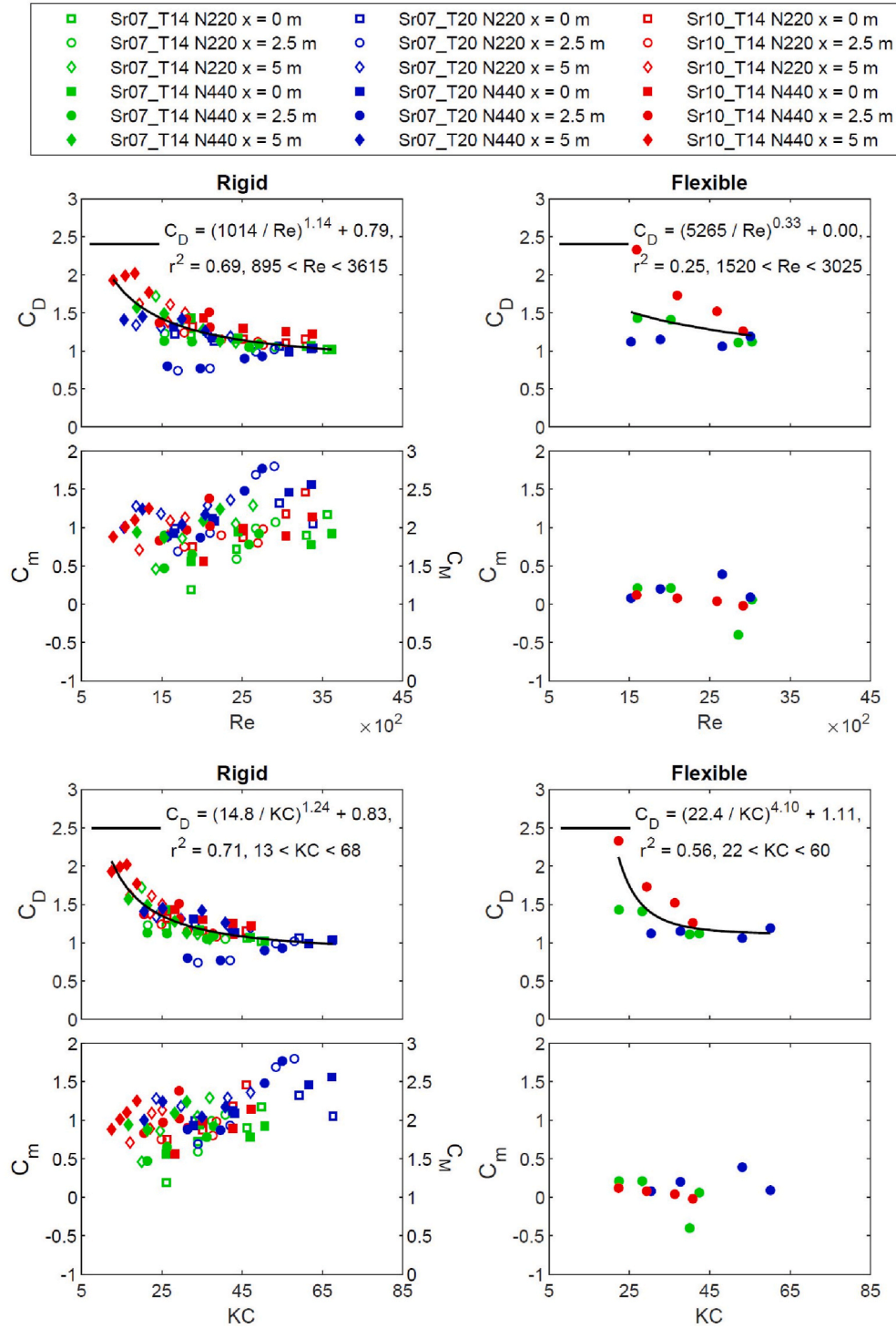
Fig. 9. C_D-*Re* and C_D-*KC* empirical relations for C_D results obtained through the LSM ($C_{D,LSM}$), along with the corresponding C_m-*Re*, C_M-*Re*, C_m-*KC*, and C_M-*KC* results for the rigid (left) and flexible (right) vegetation tests. Curve fittings (lines) of Eqs. (33) and (34) to the C_D-*Re* and C_D-*KC* results (markers) with derived equations, r^2, and ranges of *Re* and *KC*. The results related to *Re* are on top while the ones related to *KC* are at the bottom.

study results are likely due to the relatively different conditions studied.

4.3.3. C_D via least squares method

Force-related coefficients (C_D, C_m and C_M) were calculated through the least squares method (LSM) (Section 2.2) in the experimental test conditions, based on the F_{meas} (FT) and u (ADV), with a given by the variation of u (ADV) data. In the rigid near-emergent vegetation case, h_v was obtained from Eq. (7) with $h = 0.25$ m, and η given by the WG data

(Section 2.2.2). In the flexible vegetation case (Section 2.2.3) η, h_v, and u_r were given through the video analysis (Section 4.2), while a_r was obtained by the variation of the calculated u_r values in time. C_D-*Re* and C_D-*KC* empirical relations were obtained for the $C_{D,LSM}$ results (Fig. 9). Note that like for the C_D-*Re* and C_D-*KC* empirical relations obtained through the direct method (Section 4.3.2), the *Re* and *KC* calculations (Eqs. (33) and (34)), that led to the C_D-*Re* and C_D-*KC* empirical relations obtained through the LSM, considered u_c (Eq. (30)) based on the ADV
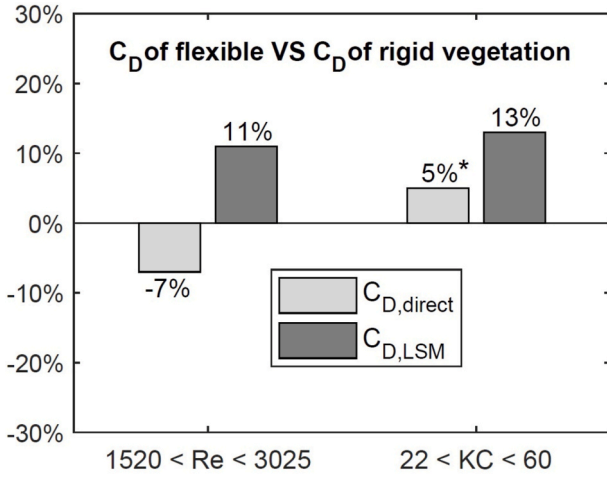
Fig. 10. Average relative differences that relate the C_D of flexible vegetation to the C_D of rigid vegetation in the obtained C_D-Re and C_D-KC relations when calculated through the direct method ($C_{D,\text{direct}}$, Fig. 8) and through the LSM ($C_{D,\text{LSM}}$, Fig. 9) within comparable Re and KC ranges.. (* due to the existence of negative and positive differences, the average was taken from the modulus of the differences.)
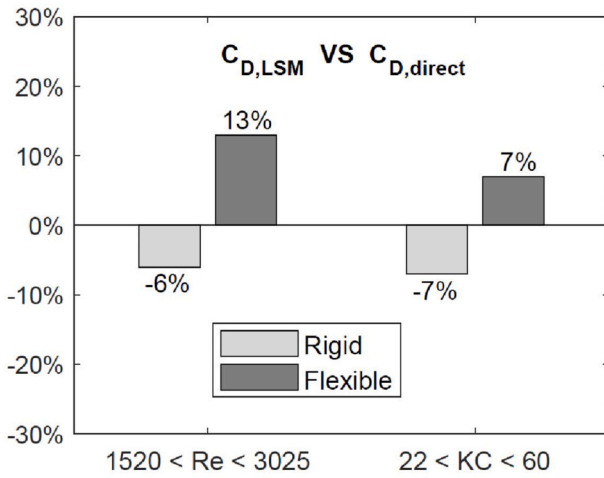

Fig. 11. Average relative differences, for rigid and flexible vegetation, that relate the C_D calculated via LSM ($C_{D,\text{LSM}}$, Fig. 9) to the C_D calculated via direct method ($C_{D,\text{direct}}$, Fig. 8) in the obtained C_D-Re and C_D-KC relations, within comparable Re and KC ranges.

data (Section 3.3).

The C_m results ranged from 0.19 ($C_M = 1.19$) to 1.80 ($C_M = 2.80$) for rigid vegetation ($895 < Re < 3615$, $13 < KC < 68$) and from -0.4 to 0.39 for flexible vegetation ($1520 < Re < 3025$, $22 < KC < 60$) (Fig. 9). Concerning the rigid vegetation case, although the C_M (and C_m) results appear dispersed, they are approximately in the range of those estimated based on force measurements for single cylinders exposed to periodic flows by Keulegan and Carpenter (1958) and Sarpkaya and Isaaction (1981). Differences may be expected since in the present study the force coefficients were estimated for in-group individual rigid cylinders exposed to waves.

4.4. C_D of flexible VS C_D of rigid vegetation

In the obtained C_D-Re and C_D-KC relations, the C_D differences found between rigid and flexible vegetation for estimations via both the direct method ($C_{D,\text{direct}}$, Fig. 8) and LSM ($C_{D,\text{LSM}}$, Fig. 9), which considered

vegetation motion (h_v, u_v, u_r, and a_r) and inertia (LSM case), suggest close C_D values for flexible and rigid plants and that C_D can be higher for flexible vegetation than for rigid vegetation within comparable KC and Re flow conditions. Note that vegetation fields with elements of the same morphology (same dimensions l_v and d_v) varying mainly in flexibility were tested (Section 3.1), favouring the comparative analysis (Fig. 10).

The obtained average difference in C_D of flexible relative to rigid vegetation was only up to 13% (Fig. 10), which is not concordant with the obtained difference in wave dissipation – 34% lower on average for flexible relative to rigid vegetation (Section 4.1). Therefore, the obtained C_D results via the direct method and LSM, which considered the vegetation swaying motion, opposed to an expected proportional relation between the difference in wave dissipation, for rigid and flexible vegetation of the same morphology, and the difference in corresponding C_D values when obtained from calibration to wave dissipation data (calibration method) without accounting for vegetation motion (van Veelen et al., 2020).

4.5. Inertia effect: C_D via LSM VS C_D via direct method

Both the direct method (Section 2.1) and the common C_D calibration to wave dissipation (calibration method) consider only the drag term of the total force exerted on the vegetation. That is based on a common assumption that the inertia force contribution to wave dissipation by vegetation is negligible, so that the work done by F_I per wave period is zero, and the work carried out by F and F_D is the same (Eq. (2)). However, in natural non-linear waves over vegetation the inertia is nonzero (Suzuki et al., 2019) and its relevance may change depending on the flexibility/motion of the vegetation.

The main difference between the C_D estimations of both utilised methods based on the force and vegetation motion – direct method ($C_{D,\text{direct}}$, Fig. 8) and LSM ($C_{D,\text{LSM}}$, Fig. 9) – is that the latter (LSM) is based on the distribution of the total force applied on the vegetation (F_{meas}) into its drag (F_D) and inertia (F_I) terms, $F_{\text{meas}} = F_D + F_I$ (Eq. (2)), estimating all force-related coefficients involved (C_D, C_m and C_M). Thus, the differences in estimated C_D results from the direct method and LSM (Fig. 11) may be attributed to the effect of inertia.

The average relative C_D difference found between the obtained $C_{D,\text{LSM}}$ (Fig. 9) and $C_{D,\text{direct}}$ (Fig. 8) relations, within comparable Re and KC ranges, was up to 13% (C_D-Re relation in flexible vegetation case). Although a generally low impact of inertia in the C_D estimation is suggested, it should be accounted (Fig. 11).

The results of relative differences between the estimated $C_{D,\text{LSM}}$ and $C_{D,\text{direct}}$ (Fig. 11) indicate that $C_{D,\text{direct}}$ (direct method) was higher than $C_{D,\text{LSM}}$ (LSM) for rigid vegetation, while $C_{D,\text{LSM}}$ was higher than $C_{D,\text{direct}}$ for flexible vegetation. Therefore, accounting for inertia reduced the C_D in rigid vegetation case and raised the C_D for flexible vegetation. Since the tested vegetation elements (same dimensions/morphology) varied mainly in flexibility (no motion vs swaying motion) the different inertia effect from rigid to flexible vegetation is likely related to the swaying motion of the flexible vegetation that was accounted for (h_v, u_v, u_r, and a_r) in the calculations. More data support would favour this conclusion.

5. Conclusions

The present study investigates the wave dissipation and the drag coefficient (C_D) for artificial rigid and flexible vegetation exposed to waves, based on flume experiments. Vegetation fields composed of mimics (cylinders) differing in Young's modulus only enabled to analyse the effect of vegetation flexural rigidity alone (flexibility as a control parameter). A video analysis was implemented to obtain data of the wave-induced swaying motion executed by an in-field target flexible cylinder (h_v and u_v).

The drag coefficient (C_D) was derived from two different methods based on force measurements: 1) the direct method and 2) the Least Squares Method (LSM). The direct method and LSM were extended to

calculate the C_D of the in-field target flexible cylinder, considering its swaying motion-related data (h_v, u_v, u_r, and a_r). The LSM considered the inertia term of the force (usually neglected), enabling to analyse the inertia effect on the C_D. The C_D results were compared between the two methods and different vegetation flexibilities for same Re and KC flow ranges.

Although the wave dissipation obtained was 34% lower on average for flexible relative to rigid vegetation, the respective C_D values for flexible and rigid vegetation, obtained from both direct method and LSM considering vegetation motion, were close. Therefore, the results found disagree with the usually observed concordance between the difference in wave dissipation for rigid and flexible vegetation and respective C_D results calculated via calibration to wave dissipation data (calibration method) without accounting for vegetation motion (e.g., van Veelen et al., 2020). Only up to a slightly higher (13% on average) C_D for flexible vegetation relative to rigid vegetation was obtained. This result also suggests that C_D for flexible vegetation can be slightly higher than for rigid vegetation.

It was found that accounting for the inertia term of the force reduced the C_D for rigid vegetation, while enhanced the C_D for flexible vegetation. This different outcome is likely related to the swaying motion only present in the flexible vegetation case. Accounting for inertia generally had a low impact (up to 13% difference on average) in the C_D results, that seems worthy of consideration and further investigation. New empirical relations between the obtained C_D results and both Re and KC numbers were formulated based on the experimental data.

This study provides methods to estimate the C_D for vegetation of different flexibilities under waves, towards a more comprehensive quantification of wave propagation over vegetation and wave-vegetation interactions. Despite harder to experimentally implement, they offer advantages compared to the common calibration method by accounting for force measurements and vegetation motion in time. Considering both drag and inertia terms of the force, the LSM is more complete. However, the direct method is more practical and applicable when inertia is negligible. It is worth noting that the present study and results are limited to the experimental conditions considered. Some common factors in natural wave vegetation exposed to waves, that were not accounted for, can significantly affect the wave dissipation and drag coefficients involved. For instance, the consideration of irregular waves, currents, wave breaking, different configuration of vegetation (distribution and density), and different vegetation flexibilities (e.g., highly flexible) are relevant in further research.

CRediT authorship contribution statement

Rui A. Reis: Writing – review & editing, Writing – original draft, Visualization, Validation, Software, Methodology, Investigation, Formal analysis, Conceptualization. **Conceição J.E.M. Fortes:** Writing – review & editing, Supervision, Resources. **José A. Rodrigues:** Writing – review & editing, Software, Formal analysis. **Zhan Hu:** Writing – review & editing, Visualization, Conceptualization. **Tomohiro Suzuki:** Writing – review & editing, Visualization, Supervision, Resources, Methodology, Conceptualization.

Declaration of competing interest

The authors declare that they have no known competing financial interests or personal relationships that could have appeared to influence the work reported in this paper.

Data availability

Data will be made available on request.

Appendix A. Supplementary data

Supplementary data to this article can be found online at https://doi.org/10.1016/j.oceaneng.2024.117002.

List of symbols

A_v	Cylinder base area [m]
a	Horizontal flow acceleration [m/s^2]
a_r	Relative horizontal acceleration between water flow and vegetation motion [m/s^2]
C_D	Drag coefficient [-]
$C_{D,direct}$	Drag coefficient calculated through the direct method [-]
$C_{D,LSM}$	Drag coefficient calculated through the least squares method [-]
C_M	Inertia coefficient [-]
C_m	Hydrodynamic-mass coefficient [-]
d_v	Cylinder diameter [m]
E	Young's elastic modulus [MPa]
EI	Flexural rigidity [N m^2]
F	Horizontal force [N]
F_D	Horizontal drag force [N]
F_I	Horizontal inertia force [N]
F_{meas}	Measured horizontal force [N]
F_{pred}	Predicted horizontal force [N]
g	Gravitational acceleration (=9.81 m/s^2) [m/s^2]
H	Wave height [m]
H_0	Wave height at the vegetation front-edge [m]
h	Still water depth [m]
h_v	Height of the cylinder underwater [m]
$h_{v,m}$	Height of the magenta marks $m = 1$ to $m = 3$ [m]
KC	Keulegan-Carpenter number [-]
l_v	Cylinder length [m]
l_v/h	Submergence ratio [-]
N_v	Vegetation spatial density [elm/m^2]
Re	Reynolds number [-]
T	Wave period [s]
t	Time [s]
u	Horizontal flow velocity [m/s]
u_c	Characteristic horizontal flow velocity [m/s]
u_r	Relative horizontal velocity between water flow and vegetation motion [m/s]
u_v	Horizontal velocity of the vegetation motion [m/s]
$u_{v,m}$	Horizontal velocity of the magenta marks $m = 1$ to $m = 3$ [m/s]
u_w	Amplitude of the horizontal wave orbital velocity [m/s]
η	Free-surface elevation [m]
ρ	Water mass density (=1000 kg/m^3) [kg/m^3]
ν	Water kinematic viscosity (=10^{-6} m^2/s) [m^2/s]

References

Anderson, M.E., Smith, J.M., McKay, S.K., 2011. Wave Dissipation by Vegetation. Technical Note ERDC/CHL CHETN-I-82. Vicksburg, MS. U.S. Army Engineer Research and Development Center.

Anderson, M.E., Smith, J.M., 2014. Wave attenuation by flexible, idealized salt marsh vegetation. Coast. Eng. 83, 82–92. https://doi.org/10.1016/j.coastaleng.2013.10.004.

Augustin, L.N., Irish, J.L., Lynett, P., 2009. Laboratory and numerical studies of wave damping by emergent and near-emergent wetland vegetation. Coast. Eng. 56, 332–340. https://doi.org/10.1016/j.coastaleng.2008.09.004.

Asano, T., Deguchi, H., Kobayashi, N., 1993. Interaction between water waves and vegetation. In: Edge, B. (Ed.), Proceedings of the Twenty-Third Coastal Engineering Conference, pp. 2710–2723.

Bouma, T.J., de Vries, M.B., Low, E., Peralta, G., Tánczos, I.C., van de Koppel, J., Herman, P.M.J., 2005. Trade-offs related to ecosystem engineering: a case study on stiffness of emerging macrophytes. Ecology 86 (8), 2187–2199. https://doi.org/10.1890/04-1588.

Bradley, K., Houser, C., 2009. Relative velocity of seagrass blades: implications forwave attenuation in low-energy environments. J. Geophys. Res. 114 (F01004), 1–13. https://doi.org/10.1029/2007JF000951.

Cao, H., Feng, W., Hu, Z., Suzuki, T., Stive, M.J.F., 2015. Numerical modeling of vegetation-induced dissipation using an extended mild-slope equation. Ocean Eng. 110, 258–269. https://doi.org/10.1016/j.oceaneng.2015.09.057.

Camfield, F., 1983. Wind-wave growth with high friction. J. Waterw. Port, Coast. Ocean Eng. 109, 115–117. https://doi.org/10.1061/(ASCE)0733-950X(1983)109:1.

Chen, H., Ni, Y., Li, Y., Liu, F., Ou, S., Su, M., Peng, Y., Hu, Z., Uijttewaal, W., Suzuki, T., 2018. Deriving vegetation drag coefficients in combined wave-current flows by calibration and direct measurement methods. Adv. Water Resour. 122, 217–227. https://doi.org/10.1016/j.advwatres.2018.10.008.

Dalrymple, R.A., Kirby, J.T., Hwang, P.A., 1984. Wave diffraction due to areas of energy dissipation. J. Waterw. Port, Coast. Ocean Eng. 110 (1), 67–79. https://doi.org/10.1061/(ASCE)0733-950X(1984)110:1(67).

Dean, R.G., Dalrymple, R.A., 1991. Water wave Mechanics for Engineers and scientists. Advanced Series on Ocean Engineering 2.

El Rahi, J., Martínez-Estévez, I., Tagliafierro, B., Domínguez, J.M., Crespo, A.J.C., Stratigaki, V., Suzuki, T., Troch, P., 2023. Numerical investigation of wave-induced flexible vegetation dynamics in 3D using a coupling between DualSPHysics and the FEA module of Project Chrono. Ocean Eng. 285 (P1), 115227 https://doi.org/10.1016/j.oceaneng.2023.115227.

Feagin, R., Irish, J., Möller, I., Williams, A., Colón-Rivera, R., 2011. Short communication: engineering properties of wetland plants with application to wave attenuation. Coast. Eng. 58 (3), 251–255.

Gijón Mancheño, A., Jansen, W., Uijttewaal, W.S.J., Reniers, A.J.H.M., van Rooijen, A.A., Suzuki, T., Etminan, V., Winterwerp, J.C., 2021. Wave transmission and drag coefficients through dense cylinder arrays: implications for designing structures for mangrove restoration. Ecol. Eng. 165, 106231.

Hu, Z., Lian, S., Zitman, T., Wang, H., He, Z., Wei, H., Ren, L., Uijttewaal, W., Suzuki, T., 2022. Wave breaking induced by opposing currents in submerged vegetation canopies. Water Resour. Res. 58 (4), e2021WR031121.

Hu, Z., Suzuki, T., Zitman, T., Uittewaal, W., Stive, M., 2014. Laboratory study on wave dissipation by vegetation in combined current–wave flow. Coast. Eng. 88, 131–142. https://doi.org/10.1016/j.coastaleng.2014.02.009.

Hunt, J.N., 1979. Direct solution of wave dispersion equation. J. Waterw. Port, Coast. Ocean Div. 105 (WW4), 457–459.

Infantes, E., Orfila, A., Bouma, T.J., Simarro, G., Terrados, J., 2011. Posidonia oceanica and Cymodocea nodosa seedling tolerance to wave exposure. Limnol. Oceanogr. 56, 2223–2232.

Jadhav, R.S., Chen, Q., Smith, J.M., 2013. Spectral distribution of wave energy dissipation by salt marsh vegetation. Coast. Eng. 77, 99–107. https://doi.org/10.1016/j.coastaleng.2013.02.013.

Keulegan, G.H., Carpenter, L.H., 1958. Forces on cylinders and plates in an oscillating fluid. J. Res. Natl. Bur. Stand. Res. Pap. 2857, 423–440.

Kobayashi, N., Raichle, A.W., Asano, T., 1993. Wave attenuation by vegetation. J. Waterw. Port, Coast. Ocean Eng. 119, 30–48. https://doi.org/10.1061/(ASCE)0733-950X(1993)119:1(30).

Koftis, T., Prinos, P., Stratigaki, V., 2013. Wave damping over artificial Posidonia oceanica meadow: a large-scale experimental study. Coast. Eng. 73, 71–83.

Luhar, M., Infantes, E., Nepf, H., 2017. Seagrass blade motion under waves and its impact on wave decay. J. Geophys. Res. Oceans 122, 3736–3752. https://doi.org/10.1002/2017JC012731.

Luhar, M., Nepf, H.M., 2016. Wave-induced dynamics of flexible blades. J. Fluid Struct. 61, 20–41. https://doi.org/10.1016/j.jfluidstructs.2015.11.007.

Luhar, M., Nepf, H.M., 2011. Flow-induced reconfiguration of buoyant and flexible aquatic vegetation. Limnol. Oceanogr. 56, 2003–2017. https://doi.org/10.4319/lo.2011.56.6.2003.

Maza, M., Lara, J.L., Losada, I.J., 2015. Tsunami wave interaction with mangrove forests: a 3-D numerical approach. Coast. Eng. 98, 33–54. https://doi.org/10.1016/j.coastaleng.2015.01.002, 2015.

Mendez, F.M., Losada, I.J., 2004. An empirical model to estimate the propagation of random breaking and nonbreaking waves over vegetation fields. Coast. Eng. 51, 103–118. https://doi.org/10.1016/j.coastaleng.2003.11.003.

Méndez, F.J., Losada, I.J., Losada, M.A., 1999. Hydrodynamics induced by wind waves in a vegetation field. J. Geophys. Res. Oceans 104, 18383–18396. https://doi.org/10.1029/1999JC900119.

Möller, I., Spencer, T., French, J., Leggett, D., Dixon, M., 1999. Wave transformation over salt marshes: a field and numerical modelling study from north Norfolk, England. Estuar. Coast Shelf Sci. 49, 411–426. https://doi.org/10.1006/ecss.1999.0509.

Morison, J.R., O'Brien, M.P., Johnson, J.W., Schaaf, S.A., 1950. The force exerted by surface waves on piles. J. Petrol. Technol. 2 (5), 149–154. https://doi.org/10.2118/950149-G.

Mullarney, J., Henderson, S., 2010. Wave-forced motion of submerged single-stem vegetation. J. Geophys. Res. Oceans 115. https://doi.org/10.1029/2010JC006448.

Nepf, H.M., 2011. In: Wolanski, E.M. (Ed.), Flow over and through Biota, Treatise on Estuarine and Coastal Science, pp. 267–288.

Ozeren, Y., Wren, D.G., Wu, W., 2014. Experimental investigation of wave attenuation through model and live vegetation. J. Waterw. Port, Coast. Ocean Eng. 140, 04014019.

Paul, M., Rupprecht, F., Möller, I., Bouma, T.J., Spencer, T., Kudella, M., Wolters, G., van Wesenbeeck, B.K., Jensen, K., Miranda-Lange, M., Schimmels, S., 2016. Plant stiffness and biomass as drivers for drag forces under extreme wave loading: a flume study on mimics. Coast. Eng. 117, 70–78. https://doi.org/10.1016/j.coastaleng.2016.07.004.

Price, W., Tomlinson, K., Hunt, J., 1968. The effect of artificial seaweed in promoting the build-up of beaches. Proceedings of 11th International Conference on Coastal Engineering 570–578. https://doi.org/10.1061/9780872620131.036.

Riffe, K.C., Henderson, S.M., Mullarney, J.C., 2011. Wave dissipation by flexible vegetation. Geophys. Res. Lett. 38, L18607 https://doi.org/10.1029/2011GL048773.

Rupprecht, F., Möller, I., Evans, B., Spencer, T., Jensen, K., 2015. Biophysical properties of salt marsh canopies - quantifying plant stem. Coast. Eng. 100, 48–57. https://doi.org/10.1016/j.coastaleng.2015.03.009.

Sánchez-González, J., Sánchez-Rojas, V., Memos, C., 2011. Wave attenuation due to Posidonia oceanica meadows. J. Hydraul. Res. 49, 503–514. https://doi.org/10.1080/00221686.2011.552464.

Sarpkaya, T., Isaacson, M., 1981. Mechanics of Wave Forces on Offshore Structures. Van Nostrand Reinhold Company.

Sumer, B.M., Fredsøe, J., 2006. Hydrodynamics Around Cylindrical Structures, Revised Edition. World Scientific.

Suzuki, T., Hu, Z., Kumada, K., Phan, L.K., Zijlema, M., 2019. Non-hydrostatic modeling of drag, inertia and porous effects in wave propagation over dense vegetation fields. Coast. Eng. 149, 49–64.

Suzuki, T., Zijlema, M., Burger, B., Meijer, M.C., Narayan, S., 2012. Wave dissipation by vegetation with layer schematization in SWAN. Coast. Eng. 59 (1), 64–71. https://doi.org/10.1016/j.coastaleng.2011.07.006.

van Veelen, T.J., Fairchild, T.P., Reeve, D.E., Karunarathna, H., 2020. Experimental study on vegetation flexibility as control parameter for wave damping and velocity structure. Coast. Eng. 157, 103648.

van Veelen, T.J., Karunarathna, H., Reeve, D.E., 2021. Modelling wave attenuation by quasi-flexible coastal vegetation. Coast. Eng. 164, 103820.

Vuik, V., Jonkman, S.N., Borsje, B.W., Suzuki, T., 2016. Nature-based flood protection: the efficiency of vegetated foreshores for reducing wave loads on coastal dikes. Coast. Eng. 116, 42–56. https://doi.org/10.1016/j.coastaleng.2016.06.001.